COMMUNICATION

Thionation induces efficient generation of excited triplet state and singlet oxygen: heavy atom-free BODIPY photosensitizers based on $S_1(n,\pi^*)$ state

Received 00th January 20xx,
Accepted 00th January 20xx

DOI: 10.1039/x0xx00000x

Wenbin Hu,[a] Xian-Fu Zhang *[b] and Mingyu Liu [a]

The attachement of SR (R is alkyl or phenyl) makes BODIPY efficiently generate excited triplet state (T_1) and singlet oxygen with quantum yield up to 0.82 (compared to 0.10 of parent BODIPY). This affords an efficient method to synthesize heavy atom free photosensitizers. This efficient T_1 formation is because SR presence leads to a new excited state $S_1(n,\pi^*)$ with an energy smaller but close to the usual $S_1(\pi,\pi^*)$ state.

The excited triplet states of organic materials have become the focus of several photoinitiated processes, such as photosensitized singlet oxygen generation for PDT (photodynamic therapy of tumor),[1-3] photochemical upconversion of near IR sunlight,[4-6] photoredox catalysis,[7-8] and singlet fission for efficient electricity generation in solar cell.[9] In many poly aromatic hydrocarbons, however, triplet excited states are often difficult to generate through direct photo-excitation owing to: (1) Intersystem crossing (ISC) from $S_1(\pi,\pi^*)$ to $T_1(\pi,\pi^*)$ is symmetrically forbidden, (2) the large singlet-triplet energy splitting in their chromophores.[10] Thus either triplet sensitization or chemical modification is used to populate triplet state. Triplet sensitization is through triplet energy transfer from a triplet donor to a target acceptor compound to efficiently access its triplet manifold of the acceptor.[11] Chemical methods to enhance the triplet formation include:

(1) Incorporation of heavy atoms into a target organic compound, such as iodine or bromine atom substitution, second- or third-row transition metal ion complexion with a target organic chromophore. This is because the spin-orbit coupling (SOC) constant is directly proportional to atomic number Z;[1, 12] (2) Appending organic electron donors to the target molecule, since photo excitation can induce the formation of charge separation state, and then charge recombination generate excited triplet state.[13]

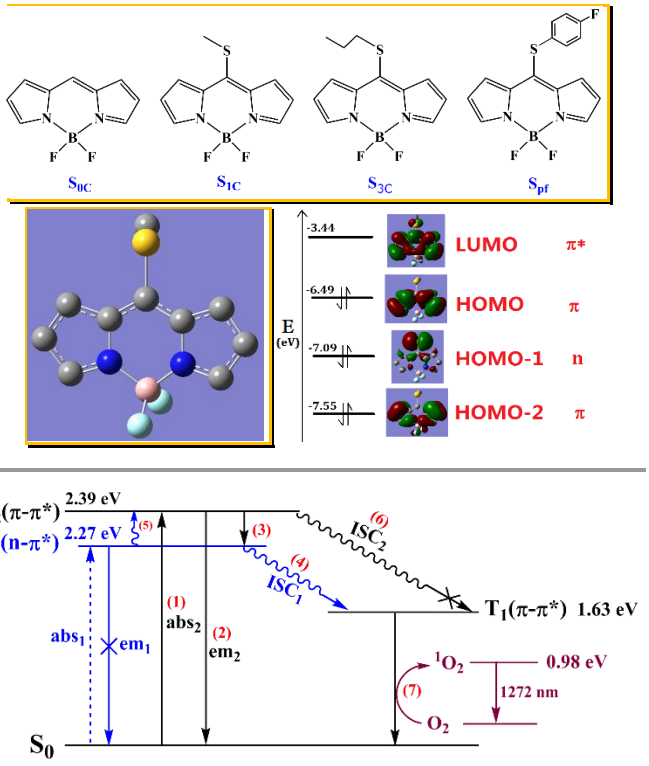

Fig. 1. Top: Chemical structures and abbreviations of SR substituted BODIPYs. **Middle**: The calculated geometry and frontier molecular orbitals for S_{1C}. **Bottom**: Mechanism that makes SR-BODIPY efficiently generate the excited triplet state; abs: absorption, em: emission, ISC: intersystem crossing.

However, heavy-atom presence also drastically shortens triplet lifetimes, while donor-acceptor architectures can be very cumbersome and tedious to design and synthesize. Another important issue is that the second- and third-row transition metals are relatively low natural abundance and requires significant cost. Therefore new methods for efficient generation of excited triplet states are highly desirable and have been under extensive investigation. Parent BODIPY $\mathbf{S_{0C}}$ is very highly fluorescent but shows low ability in generating excited triplet

[a] *Department of Chemical Engineering, Hebei Normal University of Science and Technology, Qinhuangdao, Hebei Province, China, 066004.*
[b] *MPC Technologies, Hamilton, Ontario, Canada L8S 3H4.*
Electronic Supplementary Information (ESI) available: [methods of NPs preparation, singlet oxygen detection and quantification]. See DOI: 10.1039/x0xx00000x

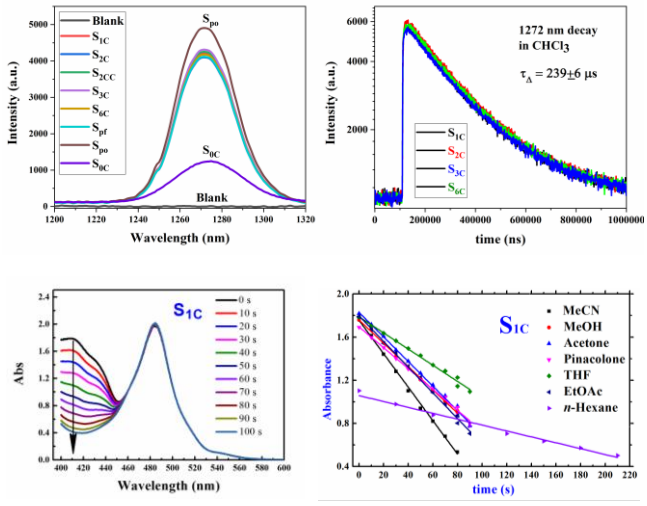

Fig. 2. Top: the NIR emission of singlet oxygen and its decay at 1272 nm in air saturated $CHCl_3$ solution of SR-BODIPY with excitation at 490 nm (absorbance 0.50). **Bottom Left**: the decrease of the DPBF absorption in the presence of S_{1C} in MeCN with irradiation at 490 nm (70 W Xenon lamp with a monochromator). **Bottom Right**: The linear dependence of DPBF absorbance at 410 nm on time.

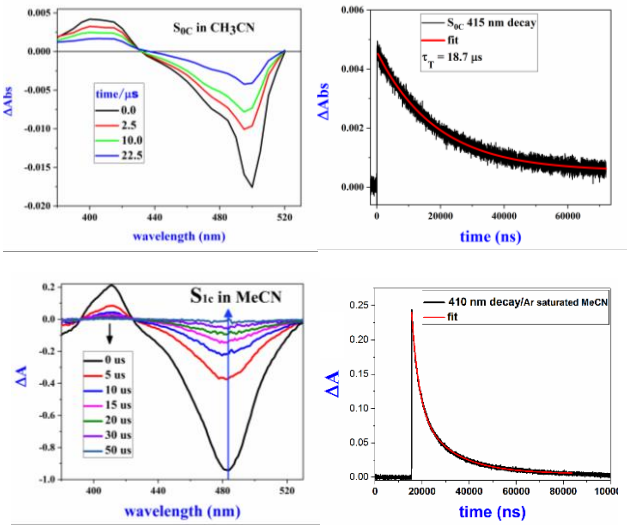

Fig. 3. Left Column: The time resolved T_1-T_n transient absorption spectra of compound S_{0C} and S_{1C} (10 μM in CH_3CN); **Right Column**: TA decay at 410 nm in Ar-saturated CH_3CN. All the solutions are excited with OPO laser at 485 nm (4 ns and ~5 mJ per pulse).

state.[14] Nevertheless, modified BODIPYS have been proposed to act as singlet oxygen photosensitizers for PDT.[15-19] We have also systematically and extensively studied how to make BODIPY generate excited triplet state T_1 efficiently by three methods: attaching an electron donor,[20-26] synthesizing BODIPY dimer,[27-29] and I/Br substitution.[30]

In this report, we show that thioalkyl or thiophenyl substitution can also lead to efficient excited triplet state formation for BODIPY compounds (Fig. 1). The mechanism for triplet formation by this method is also revealed by various methods (Fig. 1 bottom).

Table 1. Φ_Δ values in different solvents**

ε	solvent	S_{1C}	S_{3C}	S_{pf}	S_{0C}
36.6	**CH_3CN**	0.60	0.64	0.15	0.12
33. 0	**CH_3OH**	0.39	0.34	0.50	0.082
20.7	**Acetone**	0.30	0.58	0.83	0.13
12.8	**Pinacolone**	0.50	0.45	0.63	NM
7.52	**THF**	0.40	0.25	0.70	0.071
6.02	**EtOAc**	0.44	0.27	0.51	0.13
4.81	**Chloroform**	0.41	0.42	0.40	0.13
2.02	**n-hexane**	0.090	0.17	0.54	0.12

** ε: dielectrical constant of a solvent. NM=not measured.

Parent BODIPY is known to exhibit low capability to generate singlet oxygen (Table 1). In contrast, all SR-BODIPYs show much higher ability as shown in Fig. 2, in which the intensity of 1270 nm band (NIR phosphorescence of $^1O_2$) is ranked by $S_{0C} << S_{1C} \sim S_{3C} < S_{pf}$ (these spectra have been recorded under the same conditions: absorbance of an SR-BODIPY is 0.50 at excitation wavelength 490 nm in $CHCl_3$), leading to the much higher quantum yield of singlet oxygen formation (Φ_Δ in Table 1). The 1270 nm emission of the SR- BODIPYs is indeed due to $O_2(^1\Delta_g)$, since both the peak position 1270 nm and band shape, as well as the emission lifetime (239±6 μs) are all well consistent with that of reported for $O_2(^1\Delta_g)$.[31] On the other hand, if either oxygen or SR-BODIPY is absent, the 1270 nm NIR band disappears. These results imply that SR-BODIPYs indeed act as the photosensitizers of singlet oxygen.

The photosensitizing ability of the SR-BODIPYs are further demonstrated by chemical trapping, using DPBF (diphenylisobenzofuran) as the trapper of singlet oxygen. The UV-Vis absorption of DPBF (410 nm band) decreases in the co-presence of a SR-BODIPY, air and 490 nm light irradiation, during which the absorption of the SR-BODIPYs shows no change (Fig. 2 Bottom). Control experiments show that the photodecomposition of DPBF does not occur if any of SR-BODIPY, oxygen and 490 nm light irradiation is absent. The plot of absorbance at 410 nm against time is linear from which the reaction rate constant could be obtained to calculate Φ_Δ.

These SR-BODIPYs exhibit significantly high Φ_Δ up to 0.83 in various solvents (Table 1). For example, Φ_Δ of S_{pf} is 0.83, 0.70 and 0.63 in acetone, THF and pinacolone respectively; while Φ_Δ of S_{3C} is 0.64, 0.58 and 0.45 in acetonitrile, acetone and pinacolone respectively. All of which are all much higher than that of S_{0C} (0.11 in average in different solvents), clearly indicating that SR presence effectively makes BODIPYs become good singlet oxygen photosensitizer.

Next we examined if SR enhances the triplet excited state formation. Fig. 3 gives the transient absorption spectra (TAS) in acetonitrile (argon saturated) with OPO laser (4 ns pulsed) excitation at 485 nm. The TAS of S_{0C} is the same as that reported previously,[32] it is known that the positive band peaked at 410 nm is due to triplet-triplet (T_1-T_n) transient absorption, and the negative band is due to the bleaching of the ground state S_0. For S_{1C}, the shape of TAS is very similar to that of S_{0C}, except the slight red shift in peak positions. The negative absorption is assigned to the bleaching of the ground state S_0, since their band shape and position matches that of ground state S_0. The positive spectra (maxima 412 nm) are assigned to T_1 to T_n absorption, and the decrease of the positive spectra reflects the

decay of T_1 state with time ($T_1 \rightarrow S_0$). The rise of the negative band occurs concomitantly with the decrease of positive band, this is due to the regeneration of S_0 from T_1 decay ($T_1 \rightarrow S_0$), this $T_1 \rightarrow S_0$ conversion process is also supported by the presence of an isobestic point at 425 nm.

In comparison to S_{0C}, S_{1C} shows much larger absorption intensity (positive peak ΔA value in Fig. 3) in TAS under the same condition, suggesting that S_{1C} generates excited triplet state T_1 much more efficiently, i.e. SR presence very significantly enhances the excited triplet state formation. This result is consistent with the singlet oxygen measurement results. Since singlet oxygen is generated by T_1 via energy transfer: $T_1 + O_2 \rightarrow S_0 + {}^1O_2$, the more T_1 is generated, the more singlet oxygen is formed.

The triplet lifetime (τ_T) of S_{1C} and S_{3C} is obtained from the T_1 decay curve at 410 nm in argon saturated solvent (Fig. 3 right column). τ_T of S_{1C} is 15.5 μs, which is close to 18.7 μs of S_{0C}. Molecular oxygen quenches T_1 very significantly ($T_1 + O_2 \rightarrow S_0 + {}^1O_2$), since T_1 decays much faster in the presence of oxygen (supporting info), τ_T of S_{1C} and S_{0C} in air saturated solvent is 0.24 and 0.23 μs, respectively, this oxygen quenching provides a further evidence that the positive signal is due to T_1. The rate constant of the oxygen quenching (k_q) can be computed by: $\tau_T^0/\tau_T = 1+k_q\tau_T^0[O_2]$. The obtained k_q value for S_{1C} and S_{0C} is 2.05×10^9 and 2.15×10^9 $M^{-1}s^{-1}$, respectively. The large k_q values also supports that the positive signal is due to T_1.

To understand why SR presence effectively enhances T_1 and singlet oxygen formation, we have studied the related photophysical processes and calculated their electronic properties. In Fig. 4, we compare the absorption spectra of SR-BODIPYs with that of unsubstituted S_{oc}. A new absorption shoulder appears at ~513 nm for each SR-BODIPY in all solvents studied, in addition to the main peak at ~489 nm. The new peak features a weak absorption and a ~15 nm red shift relative to the main peak.

To reveal the nature of this new peak, we have performed quantum chemical calculations using time dependent density functional theory. Table 2 shows the results, together with the optimized geometry and molecular orbitals in Fig. 1. For HOMO, LUMO and HOMO-2, each orbital is delocalized over two pyrrole rings (Fig. 1), therefore they are π orbitals. For HOMO-1, however, it is almost localized on the S atom, it is therefore an n orbital. The calculated bands in Table 2 are consistent with the measured UV-Vis absorption (Fig. 4). In particular, the 512 nm band is assigned to $n \rightarrow \pi*$ transitions (97%) with a small oscillation strength of 0.018, while the main band at 485 nm is $\pi \rightarrow \pi*$ transitions (98%) with a large oscillation strength of 0.43.

Fig. 4 also compares the fluorescence emission of SR-BODIPYs with that of S_{0C}. The spectral shape of emission is similar to that of S_{0C} but the peak position is red shifted 25 nm. No new emission peaks occur, suggesting $S_1(n,\pi^*)$ is non emissive because $S_1(n,\pi^*) \rightarrow S_0(\pi,\pi^*)$ emission is symmetry forbidden. The excitation spectrum is the same as that of absorption spectrum. The fluorescence quantum yield (Φ_f), however, shows a large decrease, for example, in chloroform Φ_f of S_{0C} is 0.95, but Φ_f of S_{1C}, S_{3C}, and S_{pf} is

Table 1. The calculated first five UV-Vis absorption bands for S_{1C} in CH_3CN***

Absorption Band i	Transition Assignment	orbitals	λ_{abs} (nm)	f
Excited State 1	HOMO-1 → LUMO (97%)	n → π*	512	0.018
	HOMO → LUMO (3%)	π → π*		
Excited State 2	HOMO-2 → LUMO (10%)	π → π*	485	0.43
	HOMO → LUMO (88%)	π → π*		
	HOMO-1 → LUMO (2%)	n → π*		
Excited State 3	HOMO-1 → LUMO (90%)	n → π*	402	0.21
	HOMO → LUMO (10%)	π → π*		
Excited State 4	HOMO-2 → LUMO (99%)	π → π*	385	0.039
Excited State 5	HOMO-4 → LUMO (6%)	π → π*	297	0.18
	HOMO-3 → LUMO (91%)	π → π*		

***: λ_{abs} is the absorption maximum*1.14. f is the oscillation strength.

0.52±0.05 ns, which is about a 45% decrease. This large decrease indicates that the presence of SR causes the increase of either intersystem crossing rate constant k_{isc} or k_{ic} (internal conversion rate constant), according to following equations:

$\Phi_f = k_f/(k_f + k_{isc} + k_{ic}) = k_f\tau_f$,

$\tau_f = 1/(k_f + k_{isc} + k_{ic})$,

in which k_f and τ_f is the rate constant of radiation, and fluorescence lifetime, respectively.

SR substitution also leads to faster fluorescence decay of SR-BODIPYs than that of S_{0C}, as shown in Fig. 4 bottom, therefore SR-BODIPYs exhibit shorter fluorescence lifetime. For example, in $CHCl_3$ τ_f of S_{0C} is 7.33 ns, while τ_f of S_{1C}, S_{3C}, and S_{pf} is 5.14±0.40 ns, which is a 30% decrease. On the other hand, k_f of S_{1C}, S_{3C}, and S_{pf} (calculated by $k_f=\Phi_f/\tau_f$) is 0.11×10^9 s^{-1}, which is only slightly smaller than k_f of S_{1C} (0.13×10^9 s^{-1}).

Based on above facts, we propose the mechanism, as shown in Fig. 1 Bottom, in which the blue part drives efficient T_1 formation (ISC_1 is efficient), while the black part is the regular

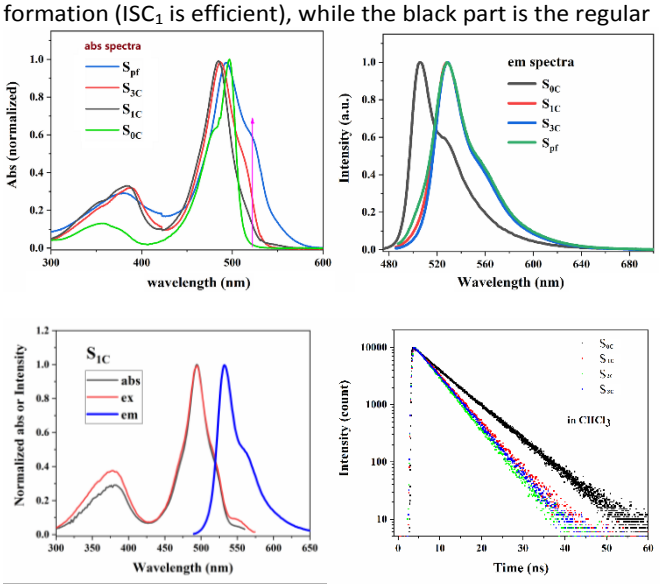

Fig. 4. **Top**: The normalized absorption and emission spectra of SR-BODIPYs. **Bottom left**: The normalized absorption, excitation and emission spectra of S_{1C}; **Bottom right**: fluorescence decay at 540 nm. **Solvent**: $CHCl_3$, sample concentration ~10 μM, excitation wavelength: 470 nm for em spectra, emission wavelength for ex spectra: 575 nm.

photophysical processes (ISC_2 is not efficient). When a *meso*-SR is attached onto the core of BODIPY, a new excited state $S_1(n,\pi^*)$ occurs, its energy is smaller but close to the usual $S_2(\pi,\pi^*)$ state (corresponding to $S_1(\pi,\pi^*)$ in parent BODIPY). Due to the forbidden symmetry, absorption abs_1 from $S_0(\pi,\pi^*)$ to $S_1(n,\pi^*)$ is fairly weak, and the emission em_1 from $S_1(n,\pi^*)$ to $S_0(\pi,\pi^*)$ does not occur. On the contrary, absorption abs_2 from $S_0(\pi,\pi^*)$ to $S_2(\pi,\pi^*)$ is strong, and the emission em_2 from $S_2(\pi,\pi^*)$ to $S_0(\pi,\pi^*)$ is symmetry allowed. $S_1(n,\pi^*)$ is mainly formed from $S_2(\pi,\pi^*)$, because $S_2(\pi,\pi^*)$ tends to relax to lower $S_1(n,\pi^*)$ to stabilize the excited molecular structure (process 3). Intersystem crossing (ISC) from $S_1(n,\pi^*)$ to $T_1(\pi,\pi^*)$ is symmetrically allowed, but ISC from $S_2(\pi,\pi^*)$ to $T_1(\pi,\pi^*)$ is symmetrically forbidden, this explains why SR enhances T_1 formation and renders BODIPY efficient photosensitizers for generating singlet oxygen. Fig. 4 shows that the intensity of $S_1(n,\pi^*)$ absorption for S_{pf} is larger than that of S_{3C} and S_{1C}, this explains why S_{pf} is more efficient in singlet oxygen formation.

We have shown that thioalkyl and thiophenyl substitution makes BODIPY become efficient photosensitizer for excited triplet state and singlet oxygen formation. This is because a new $S_1(n,\pi^*)$ state appears and has a slightly lower energy than the usual $S_1(\pi,\pi^*)$ state in S_{0C} when SR is introduced onto BODIPY core. Since Intersystem crossing (ISC) from $S_1(n,\pi^*)$ to $T_1(\pi,\pi^*)$ is symmetrically allowed, while ISC from $S_2(\pi,\pi^*)$ to $T_1(\pi,\pi^*)$ is symmetrically forbidden, this explains why SR renders BODIPY efficient photosensitizers. This fact provides a new method to efficiently generate excited triplet state and singlet oxygen without the involvement of heavy atoms for some compounds, especially BODIPY in this study. We believe this method will be helpful in developing new heavy atom free photosensitizers for photodynamic therapy, photochemical upconversion of near IR sunlight in solar cell, and photoredox catalysis.

Conflicts of interest

There are no conflicts to declare.

Notes and references

1. J. Zhao, W. Wu, J. Sun and S. Guo, *Chem. Soc. Rev.*, 2013, **42**, 5323-5351.
2. J. Zhao, K. Xu, W. Yang, Z. Wang and F. Zhong, *Chem. Soc. Rev.*, 2015, **44**, 8904-8939.
3. M. Lan, S. Zhao, W. Liu, C.-S. Lee, W. Zhang and P. Wang, *Adv. Healthcare Mater.*, 2019, **8**, 1900132.
4. T. F. Schulze and T. W. Schmidt, *Energy Environ. Sci.*, 2015, **8**, 103-125.
5. T. N. Singh-Rachford and F. N. Castellano, *Coord. Chem. Rev.*, 2010, **254**, 2560-2573.
6. Y. Y. Cheng, B. Fückel, R. W. MacQueen, T. Khoury, R. G. C. R. Clady, T. F. Schulze, N. J. Ekins-Daukes, M. J. Crossley, B. L. Stannowski, K. and T. W. Schmidt, *Energy Environ. Sci.* , 2012, **5**, 6953-6959.
7. B. D. Ravetz, A. B. Pun, E. M. Churchill, D. N. Congreve, T. Rovis and L. M. Campos, *Nature*, 2019, **565**, 343-346.
8. A. K. Pal, C. Li, G. S. Hanan and E. Zysman-Colman, *Angew. Chem., Int. Ed.*, 2018, **57**, 8027-8031.
9. J. Xia, S. N. Sanders, W. Cheng, J. Z. Low, J. Liu, L. M. Campos and T. Sun, *Adv. Mater.*, 2017, **29**, 1601652.
10. M. Montalti, A. Credi, L. Prodi and M. T. Gandolfi, *Handbook of photochemistry. 3rd ed.;*, CRC/Taylor & Francis, Boca Raton, FL, 2006.
11. T. F. Schulze and T. W. Schmidt, *Energy Environ. Sci.*, 2015, **8**, 103-125.
12. J. Zhao, S. Ji, W. Wu, W. Wu, H. Guo, J. Sun, H. Sun, Y. Liu, Q. Li and L. Huang, *RSC Adv.* , 2012, **2**, 1712-1728.
13. J. Zhao, K. Chen, Y. Hou, Y. Che, L. Liu and D. Jia, *Org. Biomol. Chem.*, 2018, **16**, 3692-3701.
14. X.-F. Zhang and J. Zhu, *J. Luminesc.*, 2019, **205**, 148-157.
15. Q. Guan, L.-L. Zhou, Y.-A. Li and Y.-B. Dong, *Chem. Commun.*, 2019, **55**, 14898-14901.
16. Y. Hou, Q. Liu and J. Zhao, *Chem. Commun.*, 2020, **56**, 1721-1724.
17. Y. Liu, C. Xu, L. Teng, H.-W. Liu, T.-B. Ren, S. Xu, X. Lou, H. Guo, L. Yua and X.-B. Zhang, *Chem. Commun.*, 2020, **56**, 1956-1959.
18. W. Wang, L. Wang, Z. Li and Z. Xie, *Chem. Commun.*, 2016, **52**, 5402-5405.
19. Y. Zhou, R. C. H. Wong, G. Dai and D. K. P. Ng, *Chem. Commun.*, 2020, **56**, 1078-1081.
20. W. Hu, M. Liu, X.-F. Zhang, Y. Wang, Y. Wang, H. Lan and H. Zhao, *J. Phys. Chem. C*, 2019, **123**, 15944-15955.
21. X.-F. Zhang and N. Feng, *Chem. Asian J.*, 2017, **12**, 2447-2456.
22. W. Hu, Y. Lin, X.-F. Zhang, M. Feng, S. Zhao and J. Zhang, *Dyes Pigm.*, 2019, **164**, 139-147.
23. X.-F. Zhang and N. Feng, *Spectrochimica Acta Part A: Molecular and Biomolecular Spectroscopy*, 2018, **189**, 13-21.
24. W. Hu, X.-F. Zhang, X. Lu, S. Lan, D. Tian, T. Li, L. Wang, S. Zhao, M. Feng and J. Zhang, *J. Luminesc.*, 2018, **194**, 185-192.
25. W. Hu, X.-F. Zhang, X. Lu, S. Lan, D. Tian, T. Li, L. Wang, S. Zhao, M. Feng and J. Zhang, *Dyes Pigm.*, 2018, **149**, 306-314.
26. X.-F. Zhang, Y. Zhang and B. Xu, *J. Photochem. Photobiol. A: Chemistry*, 2017, **349C**, 197-206.
27. X.-F. Zhang, X. Yang and B. Xu, *Phys. Chem. Chem. Phys.*, 2017, **19**, 24792-24804.
28. X.-F. Zhang, *Dyes Pigm.*, 2017, **146**, 491-501.
29. W. Pang, X.-F. Zhang, J. Zhou, C. Yu, E. Hao and L. Jiao, *Chem. Commun.*, 2012, **48**, 5437-5439
30. X.-F. Zhang, *J. Photochem. Photobiol. A: Chemistry*, 2018, **355**, 431-443.
31. E. Boix-Garriga, B. Rodríguez-Amigo, O. Planas and S. Nonell, in *Singlet Oxygen Applications in Biosciences and Nanosciences* eds. S. Nonell and C. Flors, Royal Society of Chemistry, Cambridge, 2016, p. 31.
32. X.-F. Zhang and J. Zhu, *J. Lumin.*, 2019, **212**, 286-292.